ACS OMEGA

http://pubs.acs.org/journal/acsodf

Article

Amino-Alkylphosphonate-Grafted TiO_2: How the Alkyl Chain Length Impacts the Surface Properties and the Adsorption Efficiency for Pd

Nick Gys, Rui An, Bram Pawlak, David Vogelsang, Kenny Wyns, Kitty Baert, Alexander Vansant, Frank Blockhuys, Peter Adriaensens, Tom Hauffman, Bart Michielsen, Steven Mullens, and Vera Meynen*

Cite This: *ACS Omega* 2022, 7, 45409−45421

Read Online

ACCESS | Metrics & More | Article Recommendations | Supporting Information

ABSTRACT: Amino-alkylphosphonic acid-grafted TiO_2 materials are of increasing interest in a variety of applications such as metal sorption, heterogeneous catalysis, CO_2 capture, and enzyme immobilization. To date, systematic insights into the synthesis−properties−performance correlation are missing for such materials, albeit giving important know-how towards their applicability and limitations. In this work, the impact of the chain length and modification conditions (concentration and temperature) of amino-alkylphosphonic acid-grafted TiO_2 on the surface properties and adsorption performance of palladium is studied. Via grafting with aminomethyl-, 3-aminopropyl-, and 6-aminohexylphosphonic acid, combined with the spectroscopic techniques (DRIFT, ^{31}P NMR, XPS) and zeta potential measurements, differences in surface properties between the C1, C3, and C6 chains are revealed. The modification degree decreases with increasing chain length under the same synthesis conditions, indicative of folded grafted groups that sterically shield an increasing area of binding sites with increasing chain length. Next, all techniques confirm the different surface interactions of a C1 chain compared to a C3 or C6 chain. This is in line with palladium adsorption experiments, where only for a C1 chain, the adsorption efficiency is affected by the precursor concentration used for modification. The absence of a straightforward correlation between the number of free NH_2 groups and the adsorption capacity for the different chain lengths indicates that other chain-length-specific surface interactions are controlling the adsorption performance. The increasing pH stability in the order of C1 < C3 < C6 can possibly be associated to a higher fraction of inaccessible hydrophilic sites due to the presence of folded structures. Lastly, the comparison of adsorption performance and pH stability with 3-aminopropyl(triethoxysilane)-grafted TiO_2 reveals the applicability of both grafting methods depending on the envisaged pH during sorption.

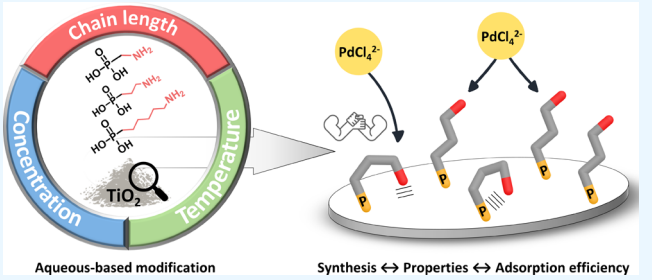

1. INTRODUCTION

Developments in non-siliceous transition-metal oxides (TiO_2, ZrO_2, Al_2O_3, ITO) are of increasing interest in various research domains.[1−3] Especially, TiO_2 is studied extensively due to its synthesis possibilities that offer a wide variety of nano-morphologies, crystal facet engineering, and the broad field of application domains such as (photo)catalysis, photovoltaic devices, and biosensing.[4−10] For several applications where the performance is governed by surface interactions, such as separation and sorption processes, the native surface chemistry (Ti−O−Ti and Ti−OH groups) limits the diversity and specificity of interactions with the environment.[11,12] Post-synthesis surface modification (i.e., grafting) with organic groups is known as a viable strategy to tune and control these surface properties given their large versatility in functional properties. Different precursors have been studied for surface grafting, such as alcohols, carboxylic acids, organosilanes, organophosphonic acids and their derivatives, and Grignard reagents.[13−15]

Although organosilanes are most widely used and well established, especially for the surface grafting of SiO_2, they are less applicable for metal oxides given their lower pH stability.[16−18] In this context, surface grafting with organo-phosphonic acids (PAs) is a promising and flexible alternative. It offers (sub)monolayer coverage with surface properties that can be controlled and tailored by changing the reaction conditions (e.g., temperature, concentration, solvent).[19−31] Especially for aliphatic PAs, such synthesis−surface properties correlations have already been studied in detail. Previous reports on propylphosphonic acid-grafted P25 concluded that the number of grafted groups, their distribution at the surface,

Received: September 17, 2022
Accepted: November 17, 2022
Published: December 1, 2022

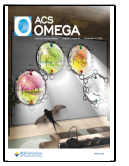

and the extent of layered titaniumalkylphosphonate formation could be tailored according to the modification conditions.[27,30]

Considering the wide versatility of PA-grafted materials, the exploration and use of PAs bearing an additional functional moiety such as amine, thiol, or carboxylic groups has received considerable attention.[32,33] In particular, most studies in this field have been devoted to the grafting with aliphatic PAs containing terminal amine functional groups given the wide-stretched application perspectives. This is evidenced by the grafting of various metal oxides including Fe_3O_4,[34−39] TiO_2,[40−46] Al_2O_3,[47,48] and ZnO,[49] targeted for applications in supported metal catalysis,[50,51] enzyme immobilization,[52] metal scavenging,[42] and hybrid (photo)electric devices.[43,53]

Besides previous reports that are mainly devoted to the application perspective, more fundamental studies focused on the various chemical states of the amine group upon grafting were also reported. Canepa et al.[54] grafted TiO_2 foils with 6-aminohexylphosphonic acid (6AHPA) and 12-aminododecylphosphonic acid (12ADDPA) and revealed the presence of both free NH_2 and protonated NH_3^+ groups via XPS analysis. Similar results were obtained on 3-aminopropylphosphonic acid (3APPA)-modified Fe_3O_4 by Tudisco et al.[36] It was suggested that the protonation of amine groups originates from the interaction of amine groups with free P−OH groups and/or through interactions with surface hydroxyl groups. Recently, a study on 3APPA-modified TiO_2 combining experimental spectroscopic techniques with DFT/PBC calculations proved the coexistence of a plethora of conformations of the aminopropyl chain on the surface, further influenced by the presence of water.[55] Since the amine functional group was found to be (partly) involved in hydrogen bonding and proton-transfer reactions, this might affect the performance in applications such as in metal sorption. However, despite the advances in amino-alkylphosphonic acid-grafted TiO_2, such correlations between the synthesis−properties and the performance have not yet been investigated. The main reason for this may be that up to now, studies from the perspective of either material characterization or performance have been carried out separately and little attention has been devoted in linking both. Nonetheless, elucidating the synthesis−properties−performance correlation is important for an improved understanding toward the viability and limitations of amino-alkylphosphonic acid-grafted TiO_2 in applications and their targeted synthesis.

This work aims to elucidate the chain-length dependence of amino-alkylphosphonic acid-grafted TiO_2 on the synthesis−properties−performance correlation using Pd adsorption as an envisaged application. Using aminomethyl-, aminopropyl-, and aminohexylphosphonic acid in combination with grafting at different concentrations and temperatures, insights are provided on the impact of the chain length on the modification degree, surface interactions at the level of the phosphonate moiety, and the chemical states of the amine functional group. Via Pd adsorption, it is evaluated to which extent the chain length and modification conditions affect the adsorption capacity, adsorption efficiency, and pH stability of the grafted groups. Next, the comparison between organophosphonic and organosilane grafting methodologies is made to reveal their distinct advantages and limitations related to the envisaged sorption conditions.

2. EXPERIMENTAL SECTION

2.1. Materials. Propylphosphonic acid (3PPA, ≥97% purity), 3-aminopropylphosphonic acid hydrochloride salt (3APPA, ≥97% purity), and 6-aminohexylphosphonic acid hydrochloride salt (6AHPA, ≥98% purity) were purchased from Sikémia. Aminomethylphosphonic acid (AMPA, 99% purity) was purchased from Alfa Aesar (Thermo Fisher Scientific). 3-Aminopropyl(triethoxysilane) (APTES) and toluene (technical grade, 98%) were purchased from Sigma-Aldrich. Molecular sieves (4 Å) were purchased from VWR. Hombikat M311, supplied by Sachtleben Chemie GmbH (now VENATOR), was used as a commercial TiO_2 support without further pre-treatment. This support consists of 100% anatase as the crystalline phase (Figure S1), has an apparent Brunauer−Emmett−Teller (BET) surface area of 300 m^2/g, and contains large mesopores/small macropores based on its nitrogen sorption isotherm and derived pore-size distribution (Figure S2). $PdCl_2$ (≥99.9%) was purchased from Sigma-Aldrich. HCl (37%, Sigma-Aldrich) and NaOH pellets (Sigma-Aldrich) were used for pH adjustments.

2.2. Surface Modification. *2.2.1. Modification with Amino-Alkylphosphonic Acids and Propylphosphonic Acid.* 2.0 g of Hombikat M311 was stirred under reflux for 4 h in a 50 mL heated aqueous solution of AMPA, 3APPA, 6AHPA, or 3PPA. Both the concentration of the PA (20, 75, and 150 mM) and temperature (50 and 90 °C) were varied. After modification, the samples were washed by pressure filtration to remove unreacted and physisorbed PA. During this process, the reactant solution was removed, followed by batch pressure filtration with 400 mL of H_2O for each washing step. After five consecutive washing steps (i.e., a total volume of 2 L), the samples were dried overnight in an oven at 60 °C. The phosphorus concentrations in the collected washing eluates were analyzed via inductively coupled plasma optical emission spectroscopy (ICP-OES) to evaluate the extent of washing (Figure S3).

All samples have been given a systematic name; the first part indicates the type of PA used, the second part represents its concentration, and the last part is the modification temperature. For example, AMPA20mM50 represents a sample modified with 20 mM of AMPA at 50 °C, while 6AHPA150mM90 represents a sample modified with 150 mM of 6AHPA at 90 °C.

2.2.2. Modification with 3-Aminopropyltriethoxysilane. 2 g of Hombikat M311 was added to a round-bottom flask, followed by addition of 200 mL of toluene dried with 4 Å molecular sieves. 19.53 mmol (3.05 mL) of 3-aminopropyltriethoxysilane was added, and the reaction mixture was stirred for 24 h under reflux (110 °C). The suspension was cooled down and filtered through a 0.4 μm cellulose filter under vacuum. The residual cake was then added to a round-bottom flask and redispersed in acetone under magnetic stirring for 2 h. The acetone suspension was filtered through a 0.4 μm cellulose filter under vacuum. This washing step was repeated once. The residual cake was then dried at 70 °C for 24 h.

2.3. Instrumentation. ICP-OES (Agilent Technologies 5100 ICP-OES) was performed to determine the phosphorus content of the AMPA, 3APPA, and 6AHPA modified samples. Samples were digested in a mixture of 1.5 mL of HNO_3 (67−69%), 1.5 mL of HF (48%), and 3 mL of H_2SO_4 (96%) for 24 h at 250 °C. After digestion, 16 mL of H_3BO_3 (4%) was added

https://doi.org/10.1021/acsomega.2c06020
ACS Omega 2022, 7, 45409−45421

to neutralize the HF. The modification degree in number of grafted groups per nm^2 (#groups/nm^2) was calculated from the weight percentage of phosphorus according to eq 1[27,56]

$$\text{mod. degr.}\left(\frac{\#}{nm^2}\right) = \frac{\text{wt \%(P)} \times N_A}{\text{MM(P)} \times S_{BET} \times 100} \quad (1)$$

in which wt % (P) is the weight percentage of phosphorus in the sample, MM (P) is the molar mass of phosphorus (g/mol), S_{BET} (nm^2/g) is the surface area of the unmodified TiO_2 powder, and N_A is Avogadro's constant (molecules/mol). The experimental error is estimated to be 0.1 groups/nm^2 based on four repeated modifications under fixed synthesis conditions.

Diffuse reflectance infrared Fourier transform (DRIFT) measurements were performed on a Nicolet 6700 Fourier Transform IR spectrometer (Thermo Scientific), equipped with an electromagnetic source in the mid-IR region (4000−700 cm^{-1}) and a DTGS detector. A resolution of 4 cm^{-1} was used, and for each spectrum, 100 scans were accumulated. The used DRIFT accessory was a Praying Mantis High Temperature Reaction Chamber (Harrick, USA) connected to a vacuum rotation pump. The sample holder contained a 4 wt % diluted sample in KBr, and measurements were performed after 30 min at room temperature under 30 mbar vacuum to reduce the amount of molecular adsorbed water. Subsequently, the samples were heated stepwise to 100 and 200 °C, followed each time by a DRIFT measurement after 30 min of equilibration time at these temperatures.

Nitrogen sorption measurements were performed at −196 °C on a Quantachrome Quadrasorb SI automated gas adsorption system. Prior to the measurements, the samples were degassed for 16 h under high vacuum at 200 °C. The specific surface area was calculated using the BET method, and the average pore size and pore size distribution were determined by the Barrett−Joyner−Halenda (BJH) method using the desorption branch.

X-ray photoelectron spectroscopy (XPS) spectra were collected using a VersaProbe II photoelectron spectroscope (Physical Electronics) with an Al Kα monochromatic X-ray source (1486.71 eV of photons). The vacuum in the analysis chamber was approximately 5×10^{-7} Pa during measurements. High-resolution scans of the Ti 2p, O 1s, C 1s, P 2p, and N 1s photoelectron peaks were recorded from a spot diameter of 100 μm using a pass energy of 23.4 eV and a step size of 0.1 eV. Measurements were performed with a take-off angle of 45° with respect to the sample surface. The powders were applied on scotch tape. Data were analyzed with CasaXPS software. Prior to curve fitting, the energy scale of the XPS spectra was calibrated relative to the binding energy of Ti 2p3/2 (458.5 eV) in $Ti(IV)O_2$.[57] Curve fitting was done after a Shirley-type background removal using mixed Gaussian−Lorentzian (80−100%) shapes for N 1s. For relative quantification of the different components in the N 1s spectra, the area of the fitted peaks was used. Two measurements were performed for each sample, and the reported percentual contributions of the N 1s components had an experimental error between 2 and 3%.

Phosphorus-31 solid-state cross-polarization magic angle spinning (CP-MAS) NMR spectra were acquired at ambient temperature on an Agilent VNMRS DirectDrive 400 MHz spectrometer (9.4 T wide bore magnet) equipped with a T3HX 3.2 mm VT probe dedicated for small sample volumes and high decoupling powers. Magic angle spinning (MAS) was performed at 15 kHz using ceramic zirconia rotors of 3.2 mm in diameter (22 μL rotors). The phosphorus chemical shift scale was calibrated to orthophosphoric acid (H_3PO_4) at 0 ppm. Other acquisition parameters used were a spectral width of 60 kHz, a 90° pulse length of 3.2 μs, a spin-lock field for CP of 80 kHz, a contact time for CP of 0.9 ms, an acquisition time of 15 ms, a recycle delay time of 4 s, and 512 accumulations. High-power proton dipolar decoupling during the acquisition time was set at 80 kHz. The Hartmann−Hahn condition for CP was calibrated accurately on the samples themselves.

Zeta potential measurements were performed on a Zetasizer Nano ZS instrument (Malvern Panalytical) equipped with a He−Ne laser (633 nm). The measurement cell consisted of a folded capillary cell of polycarbonate with gold-coated electrodes. The samples were dispersed in a 10 mM aqueous NaCl solution to maintain a constant ionic strength during pH adjustments. Dispersions were stirred continuously during pH adjustment prior to each zeta potential measurement. The reported zeta potential was the average value from three sequential measurements at each specific pH. The isoelectric point (IEP) was determined via interpolation, with the standard error based on the experimentally obtained ±1.5 mV error on the zeta potential. Diluted HCl and NaOH solutions with concentrations of 100, 10, and 1 mM were used to vary the pH. The temperature was kept constant at 25 °C.

2.4. Adsorption Experiments. For each adsorption experiment, 10 mL of Pd solution (250 mg/L) was transferred into a 20 mL closed glass vial containing 25 ± 0.5 mg of the adsorbent. The mixtures were stirred at 20 °C with a magnetic stirring bar at 300 rpm for 24 h. Next, the adsorbent was separated from the aqueous solution by filtration through a 0.45 μm syringe filter (Macherey-Nagel GmbH & Co, Germany). Then, the remaining Pd concentration in the filtrate was measured using ICP-OES (Agilent Technologies 5100). All sorption experiments were performed in duplicate. The amount of Pd adsorbed per unit mass of adsorbent at time t, q_t (mmol/g), was determined according to eq 2

$$q_t = \frac{(C_0 - C_t) \times V}{m \times \text{MM(Pd)}} \quad (2)$$

where C_0 and C_t are the initial Pd concentration (mg/L) and the concentration after adsorption for 24 h, respectively. V (L) is the volume of the solution, m (g) is the adsorbent mass, and MM(Pd) is the molar mass of palladium (i.e., 106.42 mg/mmol). For the quantification of Pd, P, and Si, the ICP-OES system was calibrated with 2% HNO_3 solutions using several calibration solutions (until 2500 μg/L) in the axial viewing direction. Independent control samples were used to check the calibration, resulting in a recovery between 90 and 110%. Multiple emission lines were measured for Pd, P, and Si to verify possible interferences. All the samples were measured in different dilutions (from 5000 to 10 times), and two of the samples were spiked.

2.5. Effect of Initial pH Value. The influence of the pH on the adsorption of Pd was studied at five different initial pH values between 1.0 ± 0.1 and 5.0 ± 0.1. Since the Pd speciation is strongly determined by the pH of the solution and concentration of chloride ions, stock solutions of Pd at pH 1 were prepared by dissolving $PdCl_2$ in 0.1 M HCl to ensure a fixed Cl^- concentration. The initial pH was adjusted using concentrated NaOH (10 M) solution or NaOH pellets. This resulted in five separate Pd solutions with a concentration of 250 mg/L, that is, one for each pH value.

https://doi.org/10.1021/acsomega.2c06020
ACS Omega 2022, 7, 45409−45421

3. RESULTS AND DISCUSSION

3.1. Impact of Concentration and Temperature on the Modification Degree. In a first step, changes in the modification degree, induced by differences in the modification conditions (i.e., concentration, temperature) and in function of the chain length of the amino-alkylphosphonic acid (i.e., AMPA, 3APPA, and 6AHPA), were evaluated (Table 1). For AMPA, modification degrees change significantly in function of the concentration as these values range between 0.9 and 1.7 #/nm^2. However, there seems to be little to no influence of the temperature taking into account the experimental error of 0.1 #/nm^2. Also for 3APPA, the modification degree increases with increasing concentration but much less pronounced than for AMPA. Furthermore, an increasing temperature provides a slight increase in the modification degree. Overall, lower modification degrees between 0.6 and 1.1 #/nm^2 are obtained, similar to earlier reported work where the comparison with propylphosphonic acid (3PPA) was made.[55] In that work, a smaller change in the modification degree for 3APPA was suggested to be caused by additional surface interactions of the amine group, such as folding of the aminopropyl chain towards the surface.

Table 1. Calculated Modification Degree Based on ICP-OES Analysis for Hombikat M311 Modified with Different Concentrations of AMPA, 3APPA, and 6AHPA in Water at 50 and 90 °C, Expressed as Number of Grafted Groups per nm^2 (#/nm^2)[a]

T (°C)	C (mM)	AMPA (#/nm^2)	3APPA (#/nm^2)	6AHPA (#/nm^2)
50	20	0.9	0.6	0.4
	75	1.3	0.7	0.5
	150	1.7	0.9	0.5
90	20	1.0	0.8	0.5
	75	1.5	0.9	0.7
	150	1.7	1.1	0.7

[a]Experimental error of 0.1 #/nm^2.

When evaluating the longest alkyl chain (i.e., 6AHPA), the lowest modification degrees are obtained as they range between 0.4 and 0.7 #/nm^2. In contrast to AMPA and 3APPA, an increasing concentration does not result in a significant increase in the modification degree, while an enhanced temperature only provides a limited increase. Similar to 3APPA, this indicates the occurrence of amine−surface interactions, in which the longer chain length of adsorbed 6AHPA might sterically block or shield a larger area of binding sites (e.g., surface hydroxyl groups, Ti centers) for other 6AHPA molecules. This could be a possible explanation for the decreasing modification degree in function of the alkyl chain length.

3.2. Surface Bonds and Surface Interactions at the Level of the Phosphonate Moiety. DRIFT analysis is performed to confirm the presence of grafted AMPA, 3APPA, and 6AHPA groups and evaluate differences in their surface binding. For the sake of clarity and without affecting the main conclusions, only the DRIFT spectra of grafted samples at a concentration of 20 mM at 50 °C are shown and discussed (Figure 1). The strong similarities with the DRIFT spectra of grafted samples at a higher concentration (150 mM) or higher temperature (90 °C) are shown in Figures S4 and S5, respectively. The presence of the aminomethyl, aminopropyl, and aminohexyl chains can be evidenced in the alkyl deformation region (1480−1400 cm^{-1}). For 3APPA- and 6AHPA-grafted samples, three signals are visible at 1412, 1448, and 1465 cm^{-1} corresponding to the methylene group bonded to the phosphonate moiety (−CH_2−P), the methylene group bonded to the NH_2 functionality (−CH_2−N), and the methylene groups bonded to adjacent carbon atoms (C−CH_2−C), respectively.[58] Only one signal at 1434 cm^{-1} is present for AMPA, in agreement with the P−CH_2−N environment.

The surface binding and interaction can be evaluated by comparing the P−O regions (1300−900 cm^{-1}). Similarities are observed in the pattern of the P−O region of 3APPA20mM50 and 6AHPA20mM50, which are characterized by a superposition of at least three absorption bands at 1116, 1042, and 990 cm^{-1}. However, for AMPA20mM50, differences are

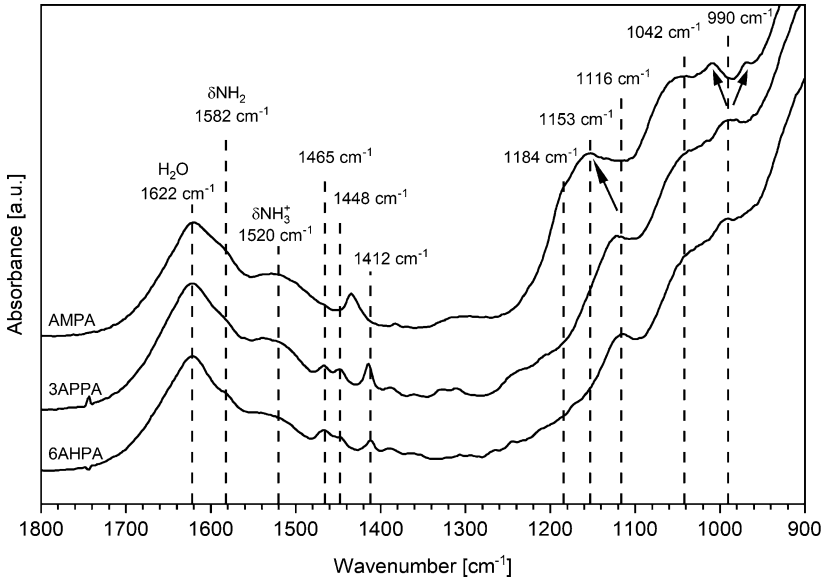

Figure 1. DRIFT spectra of AMPA20mM50, 3APPA20mM50, and 6AHPA20mM50. Offset has been used to visualize the spectra more clearly.

https://doi.org/10.1021/acsomega.2c06020
ACS Omega 2022, 7, 45409−45421

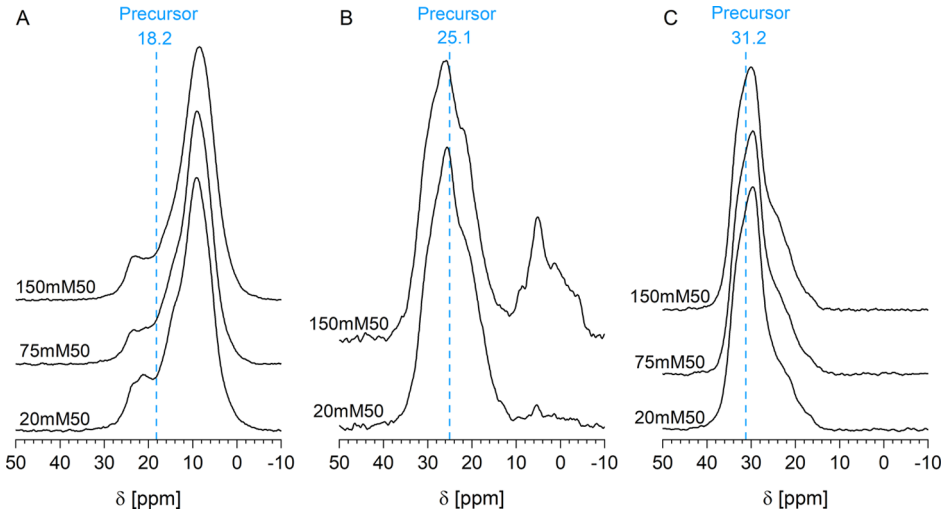

Figure 2. ^{31}P CP-MAS spectra of Hombikat grafted with AMPA (A), 3APPA (B), and 6AHPA (C) at concentrations of 20, 75, and 150 mM at 50 °C. The main position of the pure amino-alkylphosphonic acid precursor is indicated with a blue dotted line.

observed in the positions of the absorption bands and their relative intensities. Instead of the signal at 990 cm^{-1}, two absorption bands become visible at 1008 and 970 cm^{-1}. In addition, the band at 1116 cm^{-1} for 3APPA and 6AHPA is not resolved for AMPA, while two new signals become visible around 1153 and 1184 cm^{-1}. The different P−O region of AMPA-grafted samples suggests differences in its surface adsorption and associated conformations, compared to 3APPA and 6AHPA. In spite of these observations, only qualitative insights can be obtained since peak assignments to a particular conformation are difficult. Indeed, a plethora of hydrogen bonding and other non-covalent interactions are possible.

To gain further experimental insights into the surface bonding of the phosphonate moiety, solid-state ^{31}P NMR spectroscopy has been applied. Figure 2 shows the ^{31}P CP-MAS spectra of Hombikat M311 grafted with AMPA, 3APPA, and 6AHPA at concentrations of 20, 75, and 150 mM at 50 °C. Broad asymmetric signals originating from the many different chemical environments of the phosphorus atom can be associated with different binding modes and surface conformations. The AMPA-grafted samples, prepared at different concentrations, are similar in the ^{31}P NMR spectra (Figure 2A). They are characterized by a main resonance at 9.0 ppm which is clearly shifted upfield with respect to the precursor resonance signal at 18.2 ppm. In addition, a downfield shoulder between 18 and 26 ppm is present for all samples, which is composed of at least two underlying signals at 21.0 and 23.5 ppm for AMPA20mM. With increasing concentration, the relative contribution of this shoulder decreases and the 23.5 ppm signal gradually decreases in intensity until it is absent for AMPA150mM.

The ^{31}P CP-MAS spectra of 3APPA-grafted Hombikat M311 (Figure 2B) have been described in detail in previous work,[55] and only the main findings will be given here. Compared to the sharp resonance signal at 25.1 ppm of pure 3APPA (Figure S6), 3APPA20mM50 and 3APPA150mM reveal a broad envelope between 35 and 12 ppm with a main resonance signal at 25.5 ppm. These broad signals could be correlated to a wide range of intra-adsorbate, inter-adsorbate, and adsorbate−surface interactions in addition to the mono- and bidentate bonding of the phosphonic group.[55] This creates a plethora of surface conformations with each a slightly different phosphorus environment. Furthermore, 3APPA150mM shows a broad band of multiple signals between 10 and −10 ppm which can be tentatively assigned to layered titanium aminopropylphosphonate structures, formed via a dissolution−precipitation reaction.[27,59]

The pure 6AHPA precursor has a sharp resonance signal at 31.2 ppm. Similar to 3APPA, upon grafting, a broad envelope is visible between 38 and 14 ppm, but with a sharper main resonance signal at 30 ppm and an upfield shoulder centered around 22 ppm (Figure 2C). The sharper signal could indicate a relative lower diversity in surface conformations as compared to 3APPA. It can be observed that the main resonance signal of 3APPA- and 6AHPA-modified samples are only slightly shifted with 0.4 and 1.2 ppm from the resonance signal of their pure precursor, respectively. In contrast, the clear upfield shift of the main resonance for AMPA-modified samples indicates the presence of other surface interactions that distort the phosphonate environment, which is in agreement with the results from DRIFT. Such upfield shifts have previously been assigned to conformations in which the amine group is folded back towards the surface, perturbing the phosphorus environment significantly.[55] Hence, these results could hint toward a predominant presence of grafted AMPA groups with amine−surface interactions, contrary to the expectation that the short chain length of AMPA would disfavor such interactions.

3.3. Chemical State(s) of the Amine Group. Both DRIFT and XPS were used to gain insights into the chemical state(s) of the amine functionality and to which extent this was affected by the modification conditions and chain lengths. In the DRIFT spectra of AMPA20mM50, 3APPA20mM50, and 6AHPA20mM50 (Figure 1), the bending vibration of NH_2 around 1582 cm^{-1} is visible as a shoulder on the intense deformation mode of molecularly adsorbed water (1622 cm^{-1}).[60,61] In addition, in the region between 1540 and 1490 cm^{-1}, a broad absorption signal centered at 1520 cm^{-1} is present for all samples, which can be assigned to the asymmetric deformation vibration of NH_3^+ moieties.[62,63] Unfortunately, evaluating the relative contribution of the NH_2 and NH_3^+ signals for the different chain lengths is hampered due to the strong interference of adsorbed water.

https://doi.org/10.1021/acsomega.2c06020
ACS Omega 2022, 7, 45409−45421

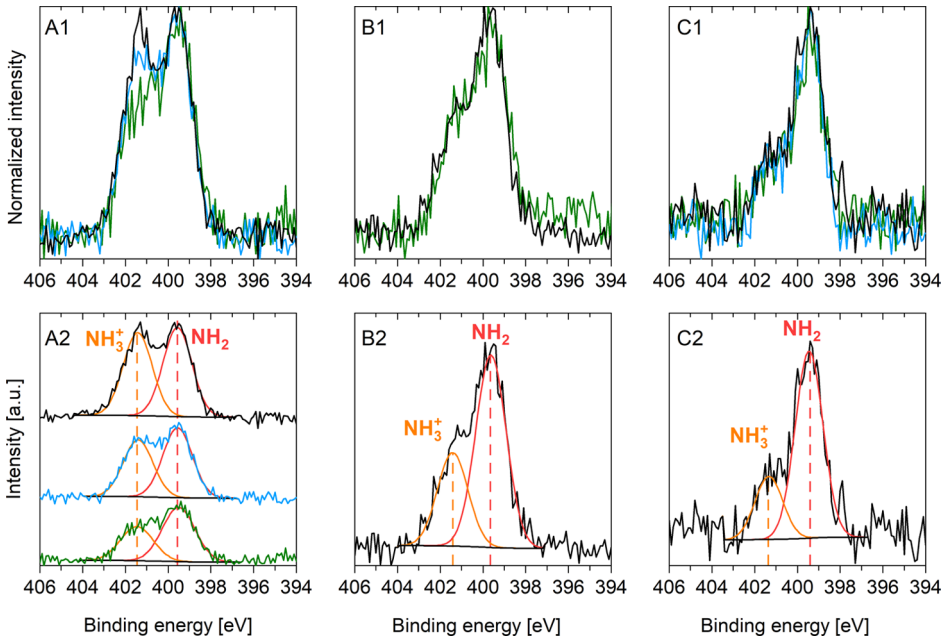

Figure 3. Normalized (first row) and peak deconvoluted (second row) N 1s spectra of AMPA (A1,A2), 3APPA (B1,B2), and 6AHPA (C1,C2) grafted Hombikat M311 at 50 °C at concentrations of 20 mM (green spectra), 75 mM (blue spectra), and 150 mM (black spectra).

Table 2. Summarizing Overview of Modification Degrees, NH_2 and NH_3^+ Percentages from XPS, Adsorption Capacities (Q_t), and Calculated Adsorption Efficiencies (Pd/N Ratio) for Hombikat M311 Grafted with AMPA, 3APPA, and 6AHPA at Concentrations of 20, 50, and 150 mM and a Temperature of 50 °C[a]

		mod. degr.	XPS (%)				
precursor	conc. (mM)	*N* (mmol/g)	NH_2	NH_3^+	NH_2(mmol/g)	Q_t(mmol/g)	Pd/N ratio
AMPA	20	0.46	62	38	0.29	0.22 ± 0.02	0.49 ± 0.03
	75	0.64	55	45	0.35	0.23 ± 0.02	0.36 ± 0.02
	150	0.82	50	50	0.41	0.22 ± 0.02	0.27 ± 0.02
3APPA	20	0.32	65	35	0.21	0.07 ± 0.01	0.21 ± 0.02
	75	0.36	65	35	0.23	0.07 ± 0.01	0.18 ± 0.03
	150	0.42	65	35	0.27	0.09 ± 0.01	0.22 ± 0.02
6AHPA	20	0.20	75	25	0.15	0.13 ± 0.01	0.66 ± 0.05
	75	0.24	75	25	0.18	0.14 ± 0.01	0.60 ± 0.04
	150	0.24	75	25	0.18	0.15 ± 0.01	0.63 ± 0.04
APTES	98	1.70	n.d.	n.d.	n.d.	0.44 ± 0.01	0.26 ± 0.01

[a]The comparison is made with an APTES-grafted sample. The Q_t values and Pd/N ratios are based on the Pd sorption experiments at pH 5 (cfr. Figure 6).

It has to be noted that DRIFT spectra taken at elevated temperatures can diminish the interference of water. Therefore, spectra were also recorded at 100 and 200 °C under vacuum (Figure S7). Upon increasing temperature, the relative intensity of the water signal decreases but remains visible at 200 °C for each chain length. Nevertheless, evaluating differences in the DRIFT spectra at elevated temperatures between the chain lengths can result in misinterpretations since changes in the hydration degree have been reported to alter the local phosphorous environments and conformations of aminopropylphosphonic acid-modified TiO_2.[55]

XPS analysis of the N 1s region reveals semi-quantitative information on the amine speciation. The N 1s spectra of the pure starting precursors are shown in Figure S8. Figure 3 depicts the N 1s spectra of the modified samples at 20, 75, and 150 mM at a temperature of 50 °C. Upon grafting, a broad asymmetric band appears in the N 1s spectra for each chain length and concentration, composed of two contributions at 399.5 eV (±0.1 eV) and 401.4 (±0.1 eV) upon peak deconvolution. The former component originates from non-interacting NH_2 groups, while the latter component can be assigned to NH_3^+ groups.[64]

The AMPA-modified samples are characterized by an increase in relative intensity of the NH_3^+ signal with increasing concentration, as visible in the overlay of the normalized N 1s spectra in Figure 3A1. This gradual increase is also visualized by the N 1s spectra of each concentration after peak deconvolution (Figure 3A2). Based on the relative areas of the fitted NH_2 and NH_3^+ components, a decrease in the NH_2/NH_3^+ ratio from 62:38 to 50:50 is found with increasing concentration from AMPA20mM50 to AMPA150mM50. The results of peak deconvolution are depicted in Table 2. As already reported for 3APPA-grafted samples in previous work[55] and shown in Figure 3B1, the normalized N 1s spectra of 3APPA20mM50 and 3APPA150mM50 overlap. This corresponds to a fixed NH_2/NH_3^+ ratio of 65:35 (±2 to 3%) upon peak deconvolution. As an example, the peak deconvoluted spectrum of 3APPA150mM50 is shown in Figure 3B2. Similar

https://doi.org/10.1021/acsomega.2c06020
ACS Omega 2022, 7, 45409−45421

to 3APPA, no significant impact of the concentration is found in the normalized N 1s spectra for the 6AHPA-modified samples at 20, 50, and 150 mM (Figure 3C1). However, one can note the smaller relative contribution of the NH_3^+ signal associated with a fixed NH_2/NH_3^+ ratio of 75:25 (±2 to 3%) compared to the shorter chain lengths. This is also clearly illustrated by comparison of the peak deconvoluted spectrum of 3APPA150mM50 (Figure 3B2) and 6AHPA150mM50 (Figure 3C2).

The aforementioned results indicate differences in the type and relative amount of specific interactions in which the amine functionality is involved and its correlation to the surface conformations for the different chain lengths. Firstly, the overlap of the normalized N 1s spectra for the different concentrations in both 3APPA and 6AHPA suggests that the relative contribution of specific surface conformations is independent of the concentrations of these precursors. However, it should be noted that this reasoning is only valid if the different surface conformations have a sufficient difference in binding energy since different surface conformations could also be associated with similar N 1s binding energies. This is further complicated by the fact that hydrogen-bonded amine groups are difficult to assign via XPS since the precise peak position and the contribution to the N 1s spectrum depends on the interaction strength. Nevertheless, the 10% lower fraction of NH_3^+ species for 6AHPA compared to 3APPA can be indicative of a lower relative amount of conformations in which the alkyl chain is folded towards the surface, enabling the formation of NH_3^+ groups. This is in agreement with the more narrow peak in ^{31}P CP-MAS NMR spectra and the smaller contribution of the upfield shifted signal with respect to the main resonance. However, surprisingly, the highest relative amount of NH_3^+ groups is found for AMPA, which suggests the presence of specific stabilizing interactions for the conformations involving NH_3^+ groups. These interactions seem to be further favored with increasing concentration (and associated increasing modification degree) given the increasing relative fraction of NH_3^+ moieties.

3.4. Zeta Potential Measurements. Zeta potential measurements on native Hombikat M311 and AMPA-, 3APPA-, and 6AHPA-modified samples provide qualitative insights on the proton-exchange properties and the accessibility of the introduced amine functionality based on the zeta potential as a function of pH. As can be observed from Figure 4, native Hombikat M311 (black squares) exhibits an IEP at 6.5. This value is in agreement with the range of literature-reported IEP values between 5 and 7 for unmodified TiO_2 powder.[65−68] The observed IEPs upon grafting with the amino-alkylphosphonic acids resemble a combination of acidic P−OH groups and alkaline NH_2 groups. Grafting with propylphosphonic (3PPA), that is, the amine-free analogue of 3APPA, results in IEPs of 5.2 and 4.3 for a precursor concentration of 20 and 150 mM, respectively (Figure 5). Since the phosphonate group (PO_3H_2) of 3PPA is the only functionality possibly affecting the zeta potential, the decrease of the IEP upon 3PPA grafting can be solely ascribed to the presence of free/unbound Brönsted acidic P−OH groups. As shown in Figure 4 for 3APPA-modified samples at 20 and 150 mM (blue curves), it appears that the modification results in little to no shift in the IEP compared to native Hombikat M311, illustrating the combined impact of P−OH and NH_2 groups on the measured zeta potential.

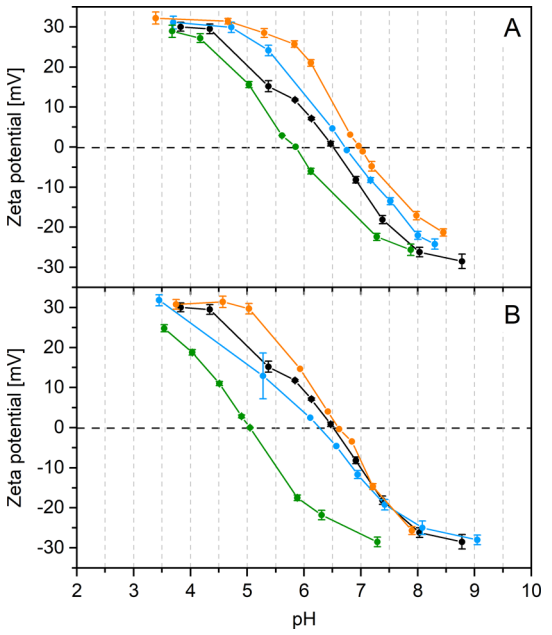

Figure 4. Zeta potential as a function of pH for native Hombikat M311 (black squares) and aminoalkyl-PA-grafted Hombikat M311 at 20mM (A) and 150 mM (B): AMPA (green), 3APPA (blue), and 6AHPA (orange). The dashed black line at ζ-potential = 0 is present to visualize the IEP more clearly.

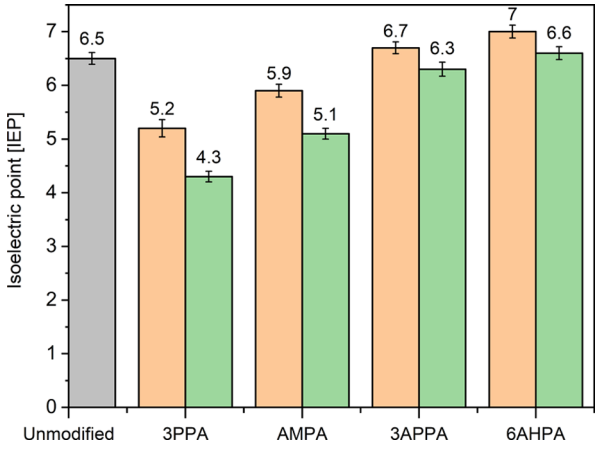

Figure 5. IEPs for unmodified Hombikat (gray), propylphosphonic acid-grafted Hombikat M311 (3PPA), and the aminoalkyl-PA-grafted samples (AMPA, 3APPA, 6AHPA). Orange- and green-colored columns represent samples grafted at 50 °C at 20 and 150 mM, respectively.

When comparing the zeta potential curves for the different chain lengths at a similar precursor concentration, a shift of the zeta potential curve to lower pH values is observed with decreasing chain length. This is also shown by the decrease of the IEPs with decreasing chain length in Figure 5. From pH titrations of the pure amino-alkylphosphonic acid precursors (Figure S9), the pK_a values of the two P−OH groups and the NH_2 group were determined (Table S1). The decreasing pK_a value from 2.3 to 1.7 of the first dissociating P−OH group with decreasing chain length could possibly contribute to the decreasing trend in IEP values. However, when acid−base groups are confined on a solid support, the effective pK_a can differ from the value obtained in the bulk liquid phase. Shyue et al.[69] obtained effective pK_a values as low as 3 for amine

https://doi.org/10.1021/acsomega.2c06020
ACS Omega 2022, 7, 45409−45421

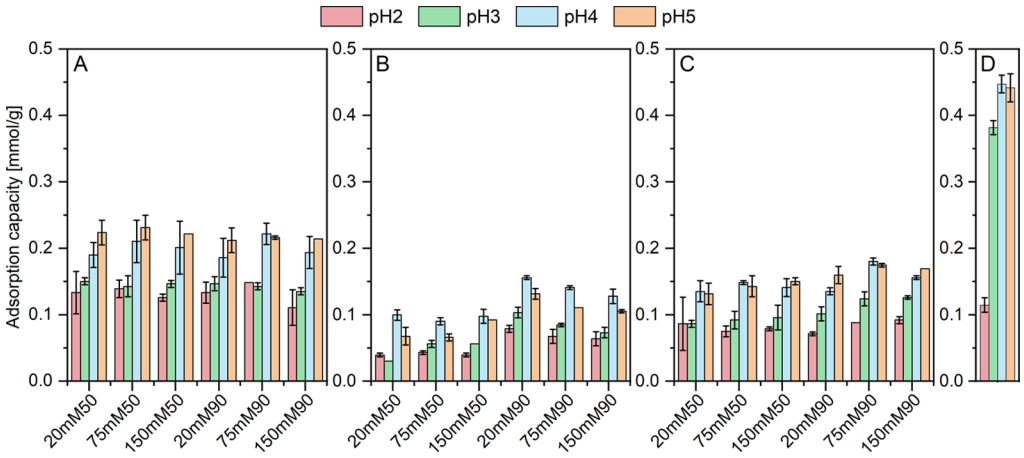

Figure 6. Effect of pH on the adsorption capacity for Pd (mmol/g) of Hombikat grafted with AMPA (A), 3APPA (B), 6AHPA (C), and APTES (D). pH = 2 (red), pH = 3 (green), pH = 4 (blue), and pH = 5 (orange). Adsorbent dose: 2.5 g/L, t = 24 h, and C_{Pd} = 250 mg/L. Under complete Pd depletion, an adsorption capacity of 0.94 mmol/g would be obtained.

groups in aminosiloxane-grafted silica. This can be explained by a protonated amine group suppressing the ionization of an adjacent neutral group, resulting in pK_a values that depend on the pH of the surrounding medium (which is not the case for amines in solution).

Given the different chemical states and interactions in which the amine groups are present at the surface (XPS), combined with the different phosphonate environments (^{31}P NMR), it is highly likely that a variety of effective dissociation constants (p$K_{a,eff}$) are present for the amine groups and P−OH groups. Combined with the macroscopic nature of zeta potential measurements, revealing an averaged surface charge, the precise individual contribution of the amine groups on the zeta potential for each precursor remains elusive.

3.5. Correlation with Palladium Sorption. Based on all data, an impact of the chain length of the amino-alkylphosphonic acid is apparent. Moreover, for AMPA, a much larger difference in surface properties can be observed in comparison to 3APPA and 6AHPA based on the ^{31}P NMR and XPS data. These differences might have an impact on the performance in application. Therefore, in order to probe the amine accessibility in an aqueous environment, that is, resembling application-related conditions, metal adsorption experiments were conducted. Pd was selected as a probe since it was reported to have a high affinity for nitrogen-based functionalities, while possessing a negligible affinity for oxygen-containing groups (e.g., Ti−OH, P−OH groups).[70,71]

At first, the impact of the pH on the adsorption capacity is studied in the pH region of 2−5 since Pd is able to form stable chloro-complexes such as $PdCl_2$, $PdCl_3^-$, and $PdCl_4^{2-}$ under these conditions.[72] The Pd speciation strongly depends on the chloride concentration and pH, and therefore, a fixed chloride concentration (0.1 M) is maintained to ensure that $PdCl_4^{2-}$ is the predominant complex at each pH (Figure S10).[73]Figure 6 plots the impact of the pH on the adsorption capacity for AMPA-, 3APPA-, and 6AHPA-grafted samples at different concentrations (20, 50, 150 mM) and temperatures (50, 90 °C). It should be noted that the initial Pd concentration of 250 mg/L is higher than in real applications to avoid the complete depletion of Pd after adsorption. The adsorption capacity for all samples is the highest at pH 4 and 5. Previous studies on the adsorption of Pd on amine-based sorbents ascribed the lower adsorption capacity at acidic pHs (2−3) to a stronger competition between chloride ions and $PdCl_4^{2-}$ on the interaction with protonated amine groups.[74,75] The adsorption mechanism can occur through an electrostatic attraction between positively charged amine groups and negatively charged $PdCl_4^{2-}$ complexes and/or via a coordinative/chelation mechanism.[76] Therefore, it is difficult to assess the prevalence of either adsorption mechanism, but it is clear that charge effects might play a role due to the lower sorption capacities at pH 2 and 3 for all materials.

For the same functional group, no difference in behavior dependent on the synthesis conditions seems to be present for the AMPA (Figure 6A) and 6AHPA samples (Figure 6C), taking into account the experimental error, except for 3APPA (Figure 6B), where a slightly higher sorption capacity is observed at 90 °C. The underlying reason remains yet to be elucidated. The APTES-grafted sample (Figure 6D) also shows a maximal adsorption capacity at pH 4 and pH 5, while revealing a much higher adsorption capacity than all PA-modified samples. The 3APPA-grafted samples seem to behave slightly different from the other PA-grafted samples as the maximal adsorption capacities are found at pH 4 and a slightly lower value is obtained at pH 5.

From an application point of view, the APTES-grafted sample would be the most viable material given the highest adsorption capacities of 0.45 mmol/g compared to AMPA ($Q_{average}$ = 0.25 mmol/g), 3APPA ($Q_{average}$ = 0.15 mmol/g), and 6AHPA ($Q_{average}$ = 0.17 mmol/g). However, from the perspective of studying the surface properties−performance correlation of phosphonic acid-modified materials, it is of importance to compare the adsorption efficiency in relation to differences in surface properties and hence amine accessibility. Therefore, the adsorption efficiency is defined as the amount of adsorbed Pd in function of the modification degree (i.e., Pd/N ratio), both expressed in mmol/g. This enables a representative comparison between samples with a different modification degree. The adsorption efficiencies are calculated based on the adsorption capacities at pH 5. An overview of the calculated adsorption efficiencies for samples modified at 20, 50, and 150 mM at 50 °C is shown in Table 2. The highest adsorption efficiencies were obtained for the 6AHPA-grafted samples (0.66−0.60), with similar calculated Pd/N ratios for each concentration within the experimental error. For AMPA-grafted samples, Pd/N ratios between 0.49 and 0.27 were

https://doi.org/10.1021/acsomega.2c06020
ACS Omega 2022, 7, 45409−45421

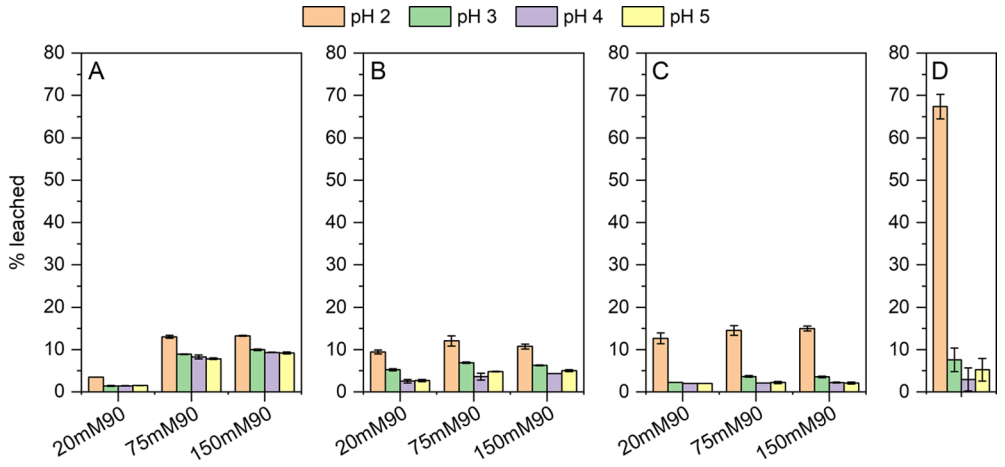

Figure 7. Leaching degree* (%) of grafted groups from AMPA (A), 3APPA (B), 6AHPA (C), and APTES (D) grafted Hombikat M311 during the Pd adsorption experiments (cfr. Figure 6). *The leaching degree was calculated based on the phosphorus and silicon concentrations in the eluates after adsorption, measured by ICP-OES.

found, characterized by a decrease in the adsorption efficiency with increasing precursor concentration. The lowest adsorption efficiencies are obtained for 3APPA-grafted samples, varying between 0.22 and 0.18. Moreover, although the higher modification degree for APTES-grafted Hombikat (i.e., 1.7 mmol/g) causes a high adsorption capacity (Figure 6), the adsorption efficiency (Pd/N) was only around 0.26, being slightly higher than that for 3APPA-grafted samples but only half of that of 6AHPA. Given the high surface coverage of amine groups for APTES, the relatively low adsorption efficiency might be (partly) ascribed to the participation of two amine groups in the adsorption of one Pd complex. Furthermore, also the formation of ring-type structures at the surface, as reported by earlier experimental and computational reports, could be responsible for the lower adsorption efficiency, herein caused by the interaction of amine groups with silanol groups.[77,78]

Based on the aforementioned results, the adsorption efficiency increases in the order of APTES ≈ 3APPA < AMPA < 6AHPA. The decrease in adsorption efficiency for AMPA with increasing concentration (i.e., increasing modification degree) seems to be associated with changes in the surface chemistry. This can encompass a combination of multiple aspects, such as changes in the adjacent distance between grafted AMPA groups possibly affecting the number of interacting amine groups for adsorption of a Pd complex (cfr. APTES) or changes in the chemical state(s) and interactions in which the amine groups are involved. Next, given the modification degree and the XPS NH_2/NH_3^+ ratios for the different chain lengths and concentrations, it is of interest to assess if the absolute number of free NH_2 groups (i.e., modification degree multiplied by the fraction of free NH_2 groups determined by XPS) correlates to the adsorbed amount of Pd (Table 2). However, no straightforward correlation can be found for the different precursors. Therefore, although XPS gives important insights into differences in chemical states of the amine functional group between different chain lengths and modification conditions, it cannot be applied to predict the adsorption performance. Clearly, other chain length-dependent interactions and properties at the surface affect the adsorption efficiency. For example, amine groups can be involved in different types and strengths of interaction (e.g., inter- and intra-adsorbate and amine−surface interactions) depending on the chain length and modification conditions, resulting in differences in the ease of breaking amine−surface interactions in favor of the interaction with a Pd complex.

3.6. pH Stability of the Grafted Amino-Alkylphosphonates and Comparison with APTES. Parallel with the Pd adsorption experiments in function of pH (Figure 6), the concentration of leached phosphorus in the eluates was measured at each pH to evaluate and compare the pH stability of grafted AMPA, 3APPA, and 6AHPA. Samples modified at the three concentrations (20, 75, and 150 mM) and at 90 °C are discussed. In addition, the comparison between 3APPA and APTES is made to assess the pH stability of an organosilane and organophosphonic acid-grafted TiO_2 surface. Figure 7 depicts the relative loss of grafted organic groups for each modification condition and chain length, defined as the relative amount of leached phosphorus (for the PAs) or silicon (for APTES) with respect to the initial amount after grafting. At pH 2, a similar range of leaching (10−15%) is found for all PA-modified materials, except for AMPA20mM90, where only a relative loss of 4% is obtained. At higher pH values, a clear decrease in the degree of leaching is visible for each chain length and concentration. Interestingly, there seems to be a correlation between the leaching percentage and the chain length. At pH values between 3 and 5, AMPA75mM90 and AMPA150mM90 exhibit a leaching between 8 and 10%, followed by 6−3% for 3APPA-grafted samples and 4−2% for 6AHPA-grafted samples.

It should be mentioned that no differences in the extent of washing after grafting between the different amino-alkylphosphonic acids are found. Therefore, the measured phosphorus concentration during pressure filtration is compared between AMPA and 6AHPA for the highest (150 mM) concentration at both 50 and 90 °C (Figure S3). When looking at the phosphorus concentration at the last washing step, that is, a total volume of 2 L, similar phosphorus concentrations between 2 and 4 mg/L are found in the eluates for both AMPA and 6AHPA. This reveals a similar extent of washing, and therefore, the observed differences in leaching degrees shown in Figure 7 are likely related to chain-length-dependent surface interactions.

These results can indicate that adsorbed AMPA possesses a lower binding strength with TiO_2 compared to 3APPA and

https://doi.org/10.1021/acsomega.2c06020
ACS Omega 2022, 7, 45409−45421

6AHPA. On the other hand, given the more hydrophilic nature of AMPA, stronger and/or more hydrophilic sites can be present at the surface, enhancing interactions with water and promoting hydrophilic attack of Ti−O−P bonds. A plausible hypothesis could be that the increasing chain length could be associated with a higher fraction of hydrophilic surface sites sterically blocked for interactions with water due to the presence of the ring-type structures. When looking at the pH stability of APTES-grafted Hombikat M311, 65−70% of the grafted groups were leached from the surface at pH 2. This also explains the low adsorption capacity for Pd at pH 2 (Figure 6). Furthermore, this illustrates the limited applicability of this grafting methodology for applications in acidic pH < 3. These results are in agreement with the lower hydrolytic stability of Ti−O−Si bonds compared to Si−O−Si bonds.[16] Several strategies can be investigated to increase the stability, such as end capping of residual Ti−OH groups or the use of amino-organosilanes with longer chain lengths to increase the hydrophobic character.

4. CONCLUSIONS

This study has been focused on unraveling the synthesis−properties−performance correlation for amino-alkylphosphonic acid-grafted TiO_2 in Pd adsorption using aminomethyl (AMPA), 3-aminopropyl (3APPA), and 6-aminohexylphosphonic acid (6AHPA). The decreasing modification degree with increasing chain length under similar synthesis conditions hints toward the presence of folded conformations (e.g., amine−surface interactions) that shield a larger area of surface binding sites. Next, AMPA reveals a peculiar behavior as it reveals the highest NH_3^+/NH_2 ratio in XPS, which also increases with increasing precursor concentration. In solid-state ^{31}P NMR, AMPA exhibits a strong upfield shift, evidencing significantly perturbed phosphorus environment(s), while the spectra of 6AHPA and 3APPA consist of a broad signal centered around the position of their pure precursor. The underlying surface interactions between AMPA and TiO_2 that are responsible for the distinct behavior of AMPA cannot yet be explained.

The impact of the chain length is also evidenced via Pd adsorption experiments, revealing an increasing adsorption efficiency (Pd/N ratio) in the order of 3APPA < AMPA < 6AHPA. While the adsorption efficiency is unaffected by the modification concentration for 3APPA and 6AHPA, AMPA shows a decreasing adsorption efficiency with increasing concentration, which might be in line with the distinct difference in synthesis−surface properties. The absence of a straightforward correlation between the number of free NH_2 groups (determined via XPS) and the adsorption capacity indicates that chain-length-dependent interaction types and strengths of the amine groups affect the possibility of interaction with Pd. While the surface coverage for AMPA is twofold and threefold higher than that for 3APPA and 6AHPA, respectively, it shows the lowest pH stability. This could be ascribed to a lower binding strength of AMPA with TiO_2 due to its higher hydrophilic nature or to the formation of more and stronger hydrophilic sites that promote the interaction with water for hydrolytic attack. In addition, although an APTES-modified sample shows a two- to threefold higher adsorption capacity than the PA-modified samples, the 65−70% leaching of grafted APTES groups at pH 2 illustrates its limited applicability under acidic conditions. This work reveals the need for further experimental and computational approaches to investigate the underlying mechanisms and the competitive interplay between amine−surface and amine−palladium interactions during adsorption.

■ ASSOCIATED CONTENT

Supporting Information

The Supporting Information is available free of charge at https://pubs.acs.org/doi/10.1021/acsomega.2c06020.

XRD data of the TiO_2 support material; N_2 physisorption data of the TiO_2 support material; evolution of the phosphorus concentration during pressure filtration; room-temperature DRIFT spectra of amino-alkylphosphonic acid-grafted TiO_2 samples, grafted at a concentration of 150 mM and a temperature of 50 °C; room-temperature DRIFT spectra of amino-alkylphosphonic acid-grafted TiO_2 samples, grafted at concentrations of 20 and 150 mM and a temperature of 90 °C; ^{31}P CP-MAS spectra of the amino-alkylphosphonic acid precursors; DRIFT spectra of amino-alkylphosphonic acid-grafted TiO_2 samples, recorded at room temperature, 100, and 200 °C; XPS N 1s spectra of the amino-alkylphosphonic acid precursors; pH titrations of the amino-alkylphosphonic acid precursors with their derived pK_a values; and impact of the chlorine concentration on the palladium speciation at pH 2 and pH 5 (PDF)

■ AUTHOR INFORMATION

Corresponding Author

Vera Meynen − *Sustainable Materials, Flemish Institute for Technological Research (VITO NV), 2400 Mol, Belgium; Laboratory of Adsorption and Catalysis (LADCA), Department of Chemistry, University of Antwerp, 2610 Wilrijk, Belgium;* orcid.org/0000-0002-9867-6986; Email: vera.meynen@uantwerpen.be

Authors

Nick Gys − *Sustainable Materials, Flemish Institute for Technological Research (VITO NV), 2400 Mol, Belgium; Laboratory of Adsorption and Catalysis (LADCA), Department of Chemistry, University of Antwerp, 2610 Wilrijk, Belgium;* Present Address: Centre for Membrane Separations, Adsorption, Catalysis and Spectroscopy (cMACS), KU Leuven, Celestijnenlaan 200F, 3001 Leuven, Belgium. Research Group Electrochemical and Surface Engineering (SURF), Vrije Universiteit Brussel, Pleinlaan 2, 1050 Brussels, Belgium; orcid.org/0000-0003-1464-6331

Rui An − *Laboratory of Adsorption and Catalysis (LADCA), Department of Chemistry, University of Antwerp, 2610 Wilrijk, Belgium*

Bram Pawlak − *Analytical and Circular Chemistry (ACC), Institute for Materials Research (IMO), Hasselt University, 3590 Diepenbeek, Belgium*

David Vogelsang − *Sustainable Materials, Flemish Institute for Technological Research (VITO NV), 2400 Mol, Belgium*

Kenny Wyns − *Sustainable Materials, Flemish Institute for Technological Research (VITO NV), 2400 Mol, Belgium;* orcid.org/0000-0003-4208-3038

Kitty Baert − *Research Group Electrochemical and Surface Engineering (SURF), Department Materials and Chemistry, Vrije Universiteit Brussel, 1050 Brussels, Belgium*

https://doi.org/10.1021/acsomega.2c06020
ACS Omega 2022, 7, 45409−45421

Alexander Vansant − *Sustainable Materials, Flemish Institute for Technological Research (VITO NV), 2400 Mol, Belgium*
Frank Blockhuys − *Structural Chemistry Group, Department of Chemistry, University of Antwerp, 2020 Antwerp, Belgium;* orcid.org/0000-0002-2201-6682
Peter Adriaensens − *Analytical and Circular Chemistry (ACC), Institute for Materials Research (IMO), Hasselt University, 3590 Diepenbeek, Belgium*
Tom Hauffman − *Research Group Electrochemical and Surface Engineering (SURF), Department Materials and Chemistry, Vrije Universiteit Brussel, 1050 Brussels, Belgium*
Bart Michielsen − *Sustainable Materials, Flemish Institute for Technological Research (VITO NV), 2400 Mol, Belgium*
Steven Mullens − *Sustainable Materials, Flemish Institute for Technological Research (VITO NV), 2400 Mol, Belgium*

Complete contact information is available at: https://pubs.acs.org/10.1021/acsomega.2c06020

Author Contributions

CRediT authorship contribution statement: N.G.: conceptualization, methodology, validation, investigation, writing—original draft, and visualization. R.A.: conceptualization, methodology, validation, investigation, writing—review and editing, and visualization. B.P. (^{31}P NMR): methodology, validation, investigation, and writing—review and editing. K.W.: validation and investigation. K.B. (XPS): methodology, validation, investigation, and visualization. A.V. (zeta potential measurements): validation and investigation. F.B.: methodology, validation, writing—review and editing, and supervision. P.A. (^{31}P NMR): methodology, writing—review and editing, and supervision. T.H. (XPS): methodology, writing—review and editing, and supervision. B.M.: conceptualization, methodology, writing—review and editing, and supervision. S.M.: conceptualization, methodology, writing—review and editing, and supervision. V.M.: conceptualization, methodology, writing—review and editing, and supervision.

Funding

This work was supported by the Research Foundation Flanders (FWO) and Hasselt University via the Hercules project AUHL/15/2-GOH3816N. B.P. acknowledges the FWO project G. 0121.17N, V.M. acknowledges FWO grant K801621N, and R.A. is grateful for the DOCPRO4 bonus project of the University of Antwerp.

Notes

The authors declare no competing financial interest.

■ ACKNOWLEDGMENTS

The authors would like to gratefully acknowledge K. Duyssens, F. Beutels, and W. Brusten for the ICP-OES measurements, J. De Wit for the pH titrations of the pure amino-alkylphosphonic acids, J. Lievens and A. Deibe Varela for assistance in the Pd sorption experiments, M. Mertens for the XRD measurements and K. Leyssens and S. Defossé for the nitrogen sorption measurements.

■ REFERENCES

(1) Gu, D.; Schüth, F. Synthesis of Non-Siliceous Mesoporous Oxides. *Chem. Soc. Rev.* **2014**, *43*, 313−344.
(2) Boyjoo, Y.; Wang, M.; Pareek, V. K.; Liu, J.; Jaroniec, M. Synthesis and Applications of Porous Non-Silica Metal Oxide Submicrospheres. *Chem. Soc. Rev.* **2016**, *45*, 6013−6047.
(3) Duan, L.; Wang, C.; Zhang, W.; Ma, B.; Deng, Y.; Li, W.; Zhao, D. Interfacial Assembly and Applications of Functional Mesoporous Materials. *Chem. Rev.* **2021**, *121*, 14349.
(4) Liu, G.; Yang, H. G.; Pan, J.; Yang, Y. Q.; Lu, G. Q. M.; Cheng, H. M. Titanium Dioxide Crystals with Tailored Facets. *Chem. Rev.* **2014**, *114*, 9559−9612.
(5) Ge, M.; Cai, J.; Iocozzia, J.; Cao, C.; Huang, J.; Zhang, X.; Shen, J.; Wang, S.; Zhang, S.; Zhang, K. Q.; Lai, Y.; Lin, Z. A Review of TiO2 Nanostructured Catalysts for Sustainable H2 Generation. *Int. J. Hydrogen Energy* **2017**, *42*, 8418−8449.
(6) Jeantelot, G.; Ould-Chikh, S.; Sofack-Kreutzer, J.; Abou-Hamad, E.; Anjum, D. H.; Lopatin, S.; Harb, M.; Cavallo, L.; Basset, J. M. Morphology Control of Anatase TiO2 for Well-Defined Surface Chemistry. *Phys. Chem. Chem. Phys.* **2018**, *20*, 14362−14373.
(7) Noman, M. T.; Ashraf, M. A.; Ali, A. Synthesis and Applications of Nano-TiO 2 : A Review. *Environ. Sci. Pollut. Res.* **2019**, *26*, 3262−3291.
(8) Katal, R.; Masudy-Panah, S.; Tanhaei, M.; Farahani, M. H. D. A.; Jiangyong, H. A Review on the Synthesis of the Various Types of Anatase TiO2 Facets and Their Applications for Photocatalysis. *Chem. Eng. J.* **2020**, *384*, 123384.
(9) Ding, Y.; Yang, I. S.; Li, Z.; Xia, X.; Lee, W. I.; Dai, S.; Bahnemann, D. W.; Pan, J. H. Nanoporous TiO2 Spheres with Tailored Textural Properties: Controllable Synthesis, Formation Mechanism, and Photochemical Applications. *Prog. Mater. Sci.* **2020**, *109*, 100620.
(10) Amri, F.; Septiani, N. L. W.; Rezki, M.; Iqbal, M.; Yamauchi, Y.; Golberg, D.; Kaneti, Y. V.; Yuliarto, B. Mesoporous TiO2-Based Architectures as Promising Sensing Materials towards next-Generation Biosensing Applications. *J. Mater. Chem. B* **2021**, *9*, 1189−1207.
(11) Mustafa, G.; Wyns, K.; Vandezande, P.; Buekenhoudt, A.; Meynen, V. Novel Grafting Method Efficiently Decreases Irreversible Fouling of Ceramic Nanofiltration Membranes. *J. Memb. Sci.* **2014**, *470*, 369−377.
(12) Florek, J.; Giret, S.; Juère, E.; Larivière, D.; Kleitz, F. Functionalization of Mesoporous Materials for Lanthanide and Actinide Extraction. *Dalton Trans.* **2016**, *45*, 14832−14854.
(13) Pujari, S. P.; Scheres, L.; Marcelis, A. T. M.; Zuilhof, H. Covalent Surface Modification of Oxide Surfaces. *Angew. Chem., Int. Ed.* **2014**, *53*, 6322−6356.
(14) Van Heetvelde, P.; Beyers, E.; Wyns, K.; Adriaensens, P.; Maes, B. U. W.; Mullens, S.; Buekenhoudt, A.; Meynen, V. A New Method to Graft Titania Using Grignard Reagents. *Chem. Commun.* **2013**, *49*, 6998−7000.
(15) Van Dijck, J. G.; Mampuys, P.; Ching, H. Y. V.; Krishnan, D.; Baert, K.; Hauffman, T.; Verbeeck, J.; Van Doorslaer, S.; Maes, B. U. W.; Dorbec, M.; Buekenhoudt, A.; Meynen, V. Synthesis − Properties Correlation and the Unexpected Role of the Titania Support on the Grignard Surface Modification. *Appl. Surf. Sci.* **2020**, *527*, 146851.
(16) Marcinko, S.; Fadeev, A. Y. Hydrolytic Stability of Organic Monolayers Supported on TiO2 and ZrO2. *Langmuir* **2004**, *20*, 2270−2273.
(17) Silverman, B. M.; Wieghaus, K. A.; Schwartz, J. Comparative Properties of Siloxane vs Phosphonate Monolayers on a Key Titanium Alloy. *Langmuir* **2005**, *21*, 225−228.
(18) Kyriakou, N.; Pizzoccaro-Zilamy, M. A.; Nijmeijer, A.; Luiten-Olieman, M.; Winnubst, L. Hydrolytic Stability of PEG-Grafted γ-Alumina Membranes: Alkoxysilane vs Phosphonic Acid Linking Groups. *Microporous Mesoporous Mater.* **2020**, *307*, 110516.
(19) Freedman, L. D.; Doak, G. O. The Preparation and Properties of Phosphonic Acids. *Chem. Rev.* **1957**, *57*, 479−523.
(20) Guerrero, G.; Mutin, P. H.; Vioux, A. Anchoring of Phosphonate and Phosphinate Coupling Molecules on Titania Particles. *Chem. Mater.* **2001**, *13*, 4367−4373.
(21) Guerrero, G.; Mutin, P. H.; Vioux, A. Organically Modified Aluminas by Grafting and Sol-Gel Processes Involving Phosphonate Derivatives. *J. Mater. Chem.* **2001**, *11*, 3161−3165.
(22) Feichtenschlager, B.; Lomoschitz, C. J.; Kickelbick, G. Tuning the Self-Assembled Monolayer Formation on Nanoparticle Surfaces

with Different Curvatures: Investigations on Spherical Silica Particles and Plane-Crystal-Shaped Zirconia Particles. *J. Colloid Interface Sci.* **2011**, *360*, 15−25.
(23) Lassiaz, S.; Labarre, D.; Galarneau, A.; Brunel, D.; Mutin, P. H. Modification of Silica by an Organic Monolayer in Aqueous Medium Using Octylphosphonic Acid and Aluminium Species. *J. Mater. Chem.* **2011**, *21*, 8199−8205.
(24) Lassiaz, S.; Galarneau, A.; Trens, P.; Labarre, D.; Mutin, H.; Brunel, D. Organo-Lined Alumina Surface from Covalent Attachment of Alkylphosphonate Chains in Aqueous Solution. *New J. Chem.* **2010**, *34*, 1424−1435.
(25) Chen, X.; Luais, E.; Darwish, N.; Ciampi, S.; Thordarson, P.; Gooding, J. J. Studies on the Effect of Solvents on Self-Assembled Monolayers Formed from Organophosphonic Acids on Indium Tin Oxide. *Langmuir* **2012**, *28*, 9487−9495.
(26) Hauffman, T.; Hubin, A.; Terryn, H. Study of the Self-Assembling of n-Octylphosphonic Acid Layers on Aluminum Oxide from Ethanolic Solutions. *Surf. Interface Anal.* **2013**, *45*, 1435−1440.
(27) Roevens, A.; Van Dijck, J. G.; Tassi, M.; D'Haen, J.; Carleer, R.; Adriaensens, P.; Blockhuys, F.; Meynen, V. Revealing the Influence of the Solvent in Combination with Temperature, Concentration and PH on the Modification of TiO2 with 3PA. *Mater. Chem. Phys.* **2016**, *184*, 324−334.
(28) Sang, L.; Knesting, K. M.; Bulusu, A.; Sigdel, A. K.; Giordano, A. J.; Marder, S. R.; Berry, J. J.; Graham, S.; Ginger, D. S.; Pemberton, J. E. Effect of Time and Deposition Method on Quality of Phosphonic Acid Modifier Self-Assembled Monolayers on Indium Zinc Oxide. *Appl. Surf. Sci.* **2016**, *389*, 190−198.
(29) Tassi, M.; Roevens, A.; Reekmans, G.; Vanhamel, M.; Meynen, V.; D'Haen, J.; Adriaensens, P.; Carleer, R. A Detailed Investigation of the Microwave Assisted Phenylphosphonic Acid Modification of P25 TiO2. *Adv. Powder Technol.* **2017**, *28*, 236−243.
(30) Roevens, A.; Van Dijck, J. G.; Geldof, D.; Blockhuys, F.; Prelot, B.; Zajac, J.; Meynen, V. Aqueous or Solvent Based Surface Modification: The Influence of the Combination Solvent − Organic Functional Group on the Surface Characteristics of Titanium Dioxide Grafted with Organophosphonic Acids. *Appl. Surf. Sci.* **2017**, *416*, 716−724.
(31) Venkata Jagadeesh, R.; Lakshminarayanan, V. Effect of Solvents on the Self-Assembly of Long Chain Alkylphosphonic Acids on Indium Tin Oxide Surface - In Situ Studies on the Adsorption Kinetics and Electron Transfer Process. *J. Electroanal. Chem.* **2019**, *835*, 338−345.
(32) Queffélec, C.; Petit, M.; Janvier, P.; Knight, D. A.; Bujoli, B. Surface Modification Using Phosphonic Acids and Esters. *Chem. Rev.* **2012**, *112*, 3777−3807.
(33) Boissezon, R.; Muller, J.; Beaugeard, V.; Monge, S.; Robin, J. J. Organophosphonates as Anchoring Agents onto Metal Oxide-Based Materials: Synthesis and Applications. *RSC Adv.* **2014**, *4*, 35690−35707.
(34) Das, M.; Mishra, D.; Maiti, T. K.; Basak, A.; Pramanik, P. Bio-Functionalization of Magnetite Nanoparticles Using an Amino-phosphonic Acid Coupling Agent: New, Ultradispersed, Iron-Oxide Folate Nanoconjugates for Cancer-Specific Targeting. *Nanotechnology* **2008**, *19*, 415101.
(35) Mohapatra, S.; Pramanik, P. Synthesis and Stability of Functionalized Iron Oxide Nanoparticles Using Organophosphorus Coupling Agents. *Colloids Surf., A* **2009**, *339*, 35−42.
(36) Tudisco, C.; Oliveri, V.; Cantarella, M.; Vecchio, G.; Condorelli, G. G. Cyclodextrin Anchoring on Magnetic Fe 3O 4 Nanoparticles Modified with Phosphonic Linkers. *Eur. J. Inorg. Chem.* **2012**, *2012*, 5323−5331.
(37) Tudisco, C.; Cambria, M. T.; Sinatra, F.; Bertani, F.; Alba, A.; Giuffrida, A. E.; Saccone, S.; Fantechi, E.; Innocenti, C.; Sangregorio, C.; Dalcanale, E.; Condorelli, G. G. Multifunctional Magnetic Nanoparticles for Enhanced Intracellular Drug Transport. *J. Mater. Chem. B* **2015**, *3*, 4134−4145.
(38) Gharbi, K.; Salles, F.; Mathieu, P.; Amiens, C.; Collière, V.; Coppel, Y.; Philippot, K.; Fontaine, L.; Montembault, V.; Smiri, L. S.; Ciuculescu-Pradines, D. Alkyl Phosphonic Acid-Based Ligands as Tools for Converting Hydrophobic Iron Nanoparticles into Water Soluble Iron-Iron Oxide Core-Shell Nanoparticles. *New J. Chem.* **2017**, *41*, 11898−11905.
(39) Tudisco, C.; Cambria, M. T.; Giuffrida, A. E.; Sinatra, F.; Anfuso, C. D.; Lupo, G.; Caporarello, N.; Falanga, A.; Galdiero, S.; Oliveri, V.; Satriano, C.; Condorelli, G. G. Comparison Between Folic Acid and GH625 Peptide-Based Functionalization of Fe3O4 Magnetic Nanoparticles for Enhanced Cell Internalization. *Nanoscale Res. Lett.* **2018**, *13*, 45.
(40) Ardalan, P.; Brennan, T. P.; Lee, H.; Bakke, J. R.; Ding, I.; McGehee, M. D.; Bent, S. F. Effects of Self-Assembled Monolayers on Solid-State CdS Quantum Dot Sensitized Solar Cells. *ACS Nano* **2011**, *5*, 1495−1504.
(41) Aquino, C. C.; Richner, G.; Chee Kimling, M.; Chen, D.; Puxty, G.; Feron, P. H. M.; Caruso, R. A. Amine-Functionalized Titania-Based Porous Structures for Carbon Dioxide Postcombustion Capture. *J. Phys. Chem. C* **2013**, *117*, 9747−9757.
(42) Seisenbaeva, G. A.; Melnyk, I. V.; Hedin, N.; Chen, Y.; Eriksson, P.; Trzop, E.; Zub, Y. L.; Kessler, V. G. Molecular Insight into the Mode-of-Action of Phosphonate Monolayers as Active Functions of Hybrid Metal Oxide Adsorbents. Case Study in Sequestration of Rare Earth Elements. *RSC Adv.* **2015**, *5*, 24575−24585.
(43) Li, X.; Ibrahim Dar, M.; Yi, C.; Luo, J.; Tschumi, M.; Zakeeruddin, S. M.; Nazeeruddin, M. K.; Han, H.; Grätzel, M. Improved Performance and Stability of Perovskite Solar Cells by Crystal Crosslinking with Alkylphosphonic Acid ω -Ammonium Chlorides. *Nat. Chem.* **2015**, *7*, 703−711.
(44) Lin, C. C.; Cho, C. P. Modified Photoanodes by Amino-Containing Phosphonate Self-Assembled Monolayers to Improve the Efficiency of Dye-Sensitized Solar Cells. *RSC Adv.* **2016**, *6*, 49702−49707.
(45) Canepa, P.; Gonella, G.; Pinto, G.; Grachev, V.; Canepa, M.; Cavalleri, O. Anchoring of Aminophosphonates on Titanium Oxide for Biomolecular Coupling. *J. Phys. Chem. C* **2019**, *123*, 16843−16850.
(46) Abate, S. Y.; Huang, D. C.; Tao, Y. T. Surface Modification of TiO2 Layer with Phosphonic Acid Monolayer in Perovskite Solar Cells: Effect of Chain Length and Terminal Functional Group. *Org. Electron.* **2020**, *78*, 105583.
(47) Ramsier, R. D.; Henriksen, P. N.; Gent, A. N. Adsorption of Phosphorus Acids on Alumina. *Surf. Sci.* **1988**, *203*, 72−88.
(48) Wapner, K.; Stratmann, M.; Grundmeier, G. Structure and Stability of Adhesion Promoting Aminopropyl Phosphonate Layers at Polymer/Aluminium Oxide Interfaces. *Int. J. Adhes. Adhes.* **2008**, *28*, 59−70.
(49) Shanmugam, N. R.; Muthukumar, S.; Prasad, S. Surface Modification of ZnO Nanostructured Electrodes with Thiol and Phosphonic Acid Moieties for Biosensing Applications. *Anal. Methods* **2017**, *9*, 5525−5533.
(50) Zhang, J.; Deo, S.; Janik, M. J.; Medlin, J. Control of Molecular Bonding Strength on Metal Catalysts with Organic Monolayers for CO2 Reduction. *J. Am. Chem. Soc.* **2020**, *142*, 5184−5193.
(51) Blanchette, Z.; Zhang, J.; Yazdi, S.; Griffin, M. B.; Schwartz, D. K.; Medlin, J. W. Investigating Deposition Sequence during Synthesis of Pd/Al 2 O 3 Catalysts Modified with Organic Monolayers. *Catal. Sci. Technol.* **2022**, *12*, 2306.
(52) Zhao, N.; Yan, L.; Zhao, X.; Chen, X.; Li, A.; Zheng, D.; Zhou, X.; Dai, X.; Xu, F. J. Versatile Types of Organic/Inorganic Nanohybrids: From Strategic Design to Biomedical Applications. *Chem. Rev.* **2019**, *119*, 1666.
(53) Fournier, O.; Bapaume, C. D.; Messou, D.; Bouttemy, M.; Schulz, P.; Ozanam, F.; Lombez, L.; Schneider, N.; Rousset, J. Chemical Passivation with Phosphonic Acid Derivatives of ZnO Deposited by Atomic Layer Deposition and Its Influence on the Halide Perovskite Interface. *ACS Appl. Energy Mater.* **2021**, *4*, 5787−5797.

https://doi.org/10.1021/acsomega.2c06020
ACS Omega 2022, 7, 45409−45421

(54) Canepa, P.; Gonella, G.; Pinto, G.; Grachev, V.; Canepa, M.; Cavalleri, O. Anchoring of Aminophosphonates on Titanium Oxide for Biomolecular Coupling. *J. Phys. Chem. C* **2019**, *123*, 16843−16850.
(55) Gys, N.; Siemons, L.; Pawlak, B.; Wyns, K.; Baert, K.; Hauffman, T.; Adriaensens, P.; Blockhuys, F.; Michielsen, B.; Mullens, S.; Meynen, V. Experimental and Computational Insights into the Aminopropylphosphonic Acid Modification of Mesoporous TiO2 Powder: The Role of the Amine Functionality on the Surface Interaction and Coordination. *Appl. Surf. Sci.* **2021**, *566*, 150625.
(56) Van Dijck, J. G.; Lenaerts, H.; Siemons, L.; Blockhuys, F.; Meynen, V. The Interaction of Water with Organophosphonic Acid Surface Modified Titania: An in-Depth in-Situ DRIFT Study. *Surface. Interfac.* **2020**, *21*, 100710.
(57) Dake, L. S.; Lad, R. J. Ultrathin Al Overlayers on Clean and K-Covered TiO 2 (110) Surfaces. *Surf. Sci. Spectra* **1996**, *4*, 232−245.
(58) Socrates, G.*Infrared and Raman Characteristic Group Frequencies*; John Wiley and Sons, Ltd, 2004.
(59) Tassi, M.; Reekmans, G.; Carleer, R.; Adriaensens, P. Fully Quantitative Description of Hybrid TiO2 Nanoparticles by Means of Solid State 31P NMR. *Solid State Nucl. Magn. Reson.* **2016**, *78*, 50−55.
(60) Paul, G.; Musso, G. E.; Bottinelli, E.; Cossi, M.; Marchese, L.; Berlier, G. Investigating the Interaction of Water Vapour with Aminopropyl Groups on the Surface of Mesoporous Silica Nanoparticles. *ChemPhysChem* **2017**, *18*, 839−849.
(61) Iliade, P.; Miletto, I.; Coluccia, S.; Berlier, G. Functionalization of Mesoporous MCM-41 with Aminopropyl Groups by Co-Condensation and Grafting: A Physico-Chemical Characterization. *Res. Chem. Intermed.* **2012**, *38*, 785−794.
(62) Sliesarenko, V. V.; Dudarko, O. A.; Zub, Y. L.; Seisenbaeva, G. A.; Kessler, V. G.; Topka, P.; Šolcová, O. One-Pot Synthesis of Mesoporous SBA-15 Containing Protonated 3-Aminopropyl Groups. *J. Porous Mater.* **2013**, *20*, 1315−1321.
(63) Zhang, L.; Liu, J.; Yang, J.; Yang, Q.; Li, C. Direct Synthesis of Highly Ordered Amine-Functionalized Mesoporous Ethane-Silicas. *Microporous Mesoporous Mater.* **2008**, *109*, 172−183.
(64) Abrahami, S. T.; Hauffman, T.; de Kok, J. M. M.; Mol, J. M. C.; Terryn, H. XPS Analysis of the Surface Chemistry and Interfacial Bonding of Barrier-Type Cr(VI)-Free Anodic Oxides. *J. Phys. Chem. C* **2015**, *119*, 19967−19975.
(65) Fazio, S.; Guzmán, J.; Colomer, M. T.; Salomoni, A.; Moreno, R. Colloidal Stability of Nanosized Titania Aqueous Suspensions. *J. Eur. Ceram. Soc.* **2008**, *28*, 2171−2176.
(66) Suttiponparnit, K.; Jiang, J.; Sahu, M.; Suvachittanont, S. Role of Surface Area, Primary Particle Size, and Crystal Phase on Titanium Dioxide Nanoparticle Dispersion Properties. *Nanoscale Res. Lett.* **2011**, *6*, 27.
(67) Sakeye, M.; Smått, J. Comparison of Di Ff Erent Amino-Functionalization Procedures on a Selection of Metal Oxide Microparticles : Degree of Modi Fi Cation and Hydrolytic Stability. *Langmuir* **2012**, *28*, 16941−16950.
(68) Zhao, J.; Milanova, M.; Warmoeskerken, M. M. C. G.; Dutschk, V. Surface Modification of TiO2nanoparticles with Silane Coupling Agents. *Colloids Surf., A* **2012**, *413*, 273−279.
(69) Shyue, J. J.; De Guire, M. R.; Nakanishi, T.; Masuda, Y.; Koumoto, K.; Sukenik, C. N. Acid-Base Properties and Zeta Potentials of Self-Assembled Monolayers Obtained via in Situ Transformations. *Langmuir* **2004**, *20*, 8693−8698.
(70) Sharma, S.; Krishna Kumar, A. S.; Rajesh, N. A Perspective on Diverse Adsorbent Materials to Recover Precious Palladium and the Way Forward. *RSC Adv.* **2017**, *7*, 52133−52142.
(71) Zheng, H.; Ding, Y.; Wen, Q.; Liu, B.; Zhang, S. Separation and Purification of Platinum Group Metals from Aqueous Solution: Recent Developments and Industrial Applications. *Resour. Conserv. Recycl.* **2021**, *167*, 105417.
(72) Colombo, C.; Oates, C. J.; Monhemius, A. J.; Plant, J. A. Complexation of Platinum, Palladium and Rhodium with Inorganic Ligands in the Environment. *Geochem. Explor. Environ. Anal.* **2008**, *8*, 91−101.
(73) Folens, K.; Van Hulle, S.; Vanhaecke, F.; Du Laing, G. Chemical Fractionation and Speciation Modelling for Optimization of Ion-Exchange Processes to Recover Palladium from Industrial Wastewater. *Water Sci. Technol.* **2016**, *73*, 1738−1745.
(74) Kramer, J.; Driessen, W. L.; Koch, K. RR. J.; Reedijk, J. Highly Selective Extraction of Platinum Group Metals with Silica-Based-(Poly) Amine Ion Exchangers Applied to Industrial Metal Refinery Effluents. *Hydrometallurgy* **2002**, *64*, 59−68.
(75) Rock, W.; Oruc, M. E.; Ellis, R. J.; Uysal, A. Molecular Scale Description of Anion Competition on Amine-Functionalized Surfaces. *Langmuir* **2016**, *32*, 11532−11539.
(76) Mincke, S.; Asere, T. G.; Verheye, I.; Folens, K.; Vanden Bussche, F.; Lapeire, L.; Verbeken, K.; Van Der Voort, P.; Tessema, D. A.; Fufa, F.; Du Laing, G.; Stevens, C. V. Functionalized Chitosan Adsorbents Allow Recovery of Palladium and Platinum from Acidic Aqueous Solutions. *Green Chem.* **2019**, *21*, 2295−2306.
(77) Marcoen, K.; Gauvin, M.; De Strycker, J.; Terryn, H.; Hauffman, T. Molecular Characterization of Multiple Bonding Interactions at the Steel Oxide-Aminopropyl Triethoxysilane Interface by ToF-SIMS. *ACS Omega* **2020**, *5*, 692−700.
(78) Meroni, D.; Lo Presti, L.; Di Liberto, G.; Ceotto, M.; Acres, R. G.; Prince, K. C.; Bellani, R.; Soliveri, G.; Ardizzone, S. A Close Look at the Structure of the TiO2-APTES Interface in Hybrid Nanomaterials and Its Degradation Pathway: An Experimental and Theoretical Study. *J. Phys. Chem. C* **2017**, *121*, 430−440.

https://doi.org/10.1021/acsomega.2c06020
ACS Omega 2022, 7, 45409−45421